INTERNATIONAL JOURNAL OF CLIMATOLOGY
Int. J. Climatol. **28**: 243–254 (2008)
Published online 29 May 2007 in Wiley InterScience
(www.interscience.wiley.com) DOI: 10.1002/joc.1528

RMetS
ROYAL METEOROLOGICAL SOCIETY

Historical trends and future predictions of climate variability in the Brahmaputra basin

Walter Immerzeel*
FutureWater, www.futurewater.nl

ABSTRACT: An innovative approach is developed and presented to assess historical climate variations and to quantify future climate change for the entire Brahmaputra basin. Historical trends in temperature and precipitation are analysed from 1900 to 2002 for the Tibetan plateau (TP), the Himalayan belt and the floodplains (FP) using a global 100 year monthly high resolution dataset. Temperature patterns are consistent with global warming and out of the 10% warmest years from 1900 to 2002 six occurred between 1995 and 2002. No clear trends in precipitation were found and annual precipitation in the basin is mainly determined by the strength of the monsoon. Regression analysis is used to further explain monsoon precipitation. A significant inverse relation is found between air temperature differences between the FP and the TP and the strength of the monsoon, whereas the El Niño Southern Oscillation teleconnection does not have a prominent role in explaining variation in monsoon precipitation. Simulation results of six general circulation models are statistically downscaled to the spatial resolution of the observed dataset for two future storylines. The analysis predicts accelerated seasonal increases in both temperature and precipitation from 2000 to 2100. The largest changes occur on the TP and the smallest on the FP. Multiple regression analysis shows a sharp increase in the occurrence of average and extreme downstream discharges for both storylines. The strongest increases are projected for the monsoon season and the largest threat of climate change lies in the associated flooding in the densely populated FP. Copyright © 2007 Royal Meteorological Society

KEY WORDS climate change; hydrology; himalaya; downscaling; flooding; ENSO

Received 6 June 2006; Revised 5 February 2007; Accepted 22 February 2007

1. Introduction

It is predicted that climate change will lead to an intensification of the global hydrological cycle and can have major impacts on regional water resources (Arnell, 1999). Changes in the total amount of precipitation and in its frequency and intensity directly affect the magnitude and timing of run-off and the intensity of floods and droughts. However, at present, specific regional effects are uncertain (IPCC, 2001).

The Himalayan range and the Tibetan plateau (TP) are the source of major river systems in Asia. The impact of climate change on the water resources of the region will be significant. Increases in evapotranspiration (ET) combined with regional changes in precipitation characteristics have the potential to affect mean run-off, frequency, and intensity of floods and droughts. Run-off in the Himalayas for example is affected by snow cover, the monsoon and cyclones. All of which may be affected by climate change (IPCC, 2001).

This study is focusing on the Brahmaputra basin originating mainly in the eastern part of the Himalayas (Figure 1). The Brahmaputra is a major transboundary river and drains an area of around 530 000 km^2. The basin is located within four different countries: China (50.5%), India (33.6%), Bangladesh (8.1%) and Bhutan (7.8%). The Brahmaputra springs from a glacier in the Kailash range in Tibet (China) at an elevation of 5300 meters above sea level (m.a.s.l.), has a length of 2900 km and after its confluence with the Ganges, the Brahmaputra flows into the Bay of Bengal. Average discharge of the Brahmaputra is approximately 20 000 m^3/s. The climate of the basin is monsoon driven with a distinct wet season from June to September, which accounts for 60–70% of the annual rainfall.

Three physiographic zones are distinguished in this study, because it is expected that each of these three physiographic units will respond differently to the anticipated climate change. First of all, the TP, covering 44.4% of the basin, with elevations of 3500 m and above in the north of the basin. Secondly the Himalaya belt (HB), covering 28.6% of the basin, with elevations ranging from 100 m.a.s.l. to 3500 m.a.s.l. Finally the agricultural floodplains (FP), covering 27.0% of the basin, of India and Bangladesh with elevation up to 100 m.a.s.l., of which 40% is flood prone.

Figure 2 shows the seasonal climate normals from 1961 to 1990 for the TP, the HB and the FP in a box-whisker plot. The plot shows the median, the upper and lower quartiles and the caps at the end of the box show the minimum and maximum. The TP is the coldest with

* Correspondence to: Walter Immerzeel, Costerweg 1G, 6702 AA Wageningen, The Netherlands.
E-mail: w.immerzeel@futurewater.nl

Copyright © 2007 Royal Meteorological Society

WILEY InterScience® DISCOVER SOMETHING GREAT

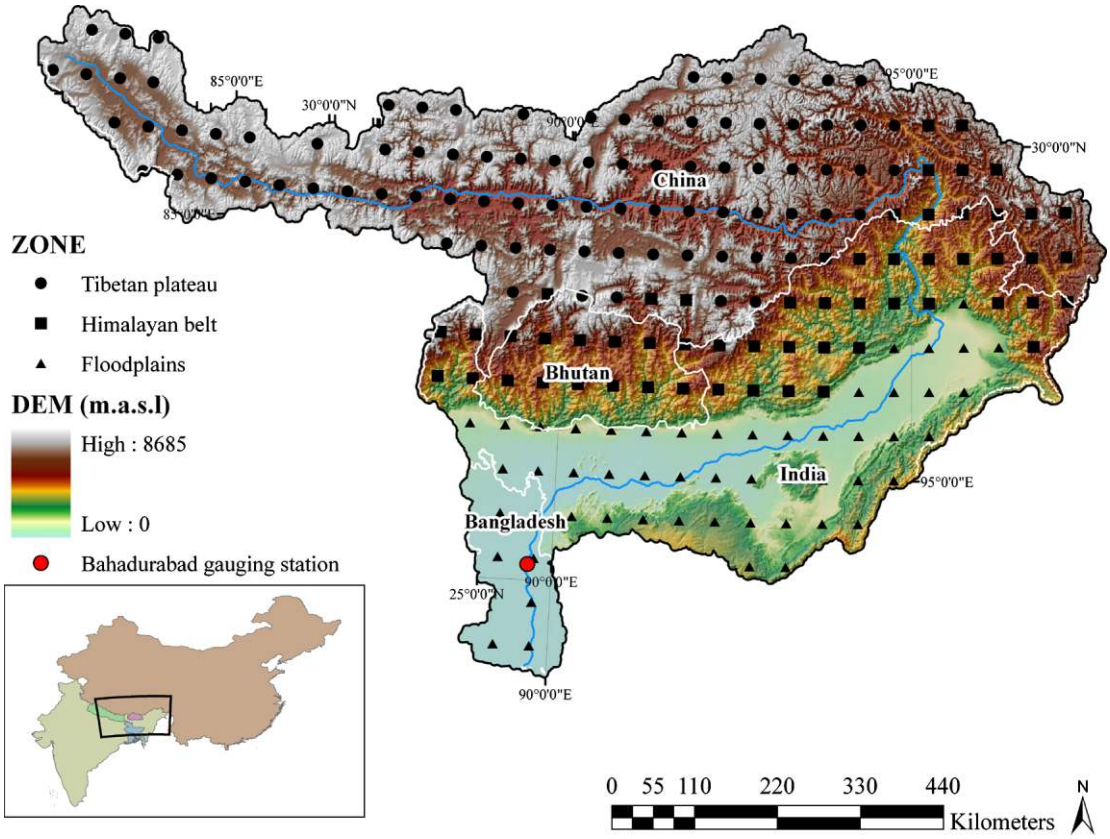

Figure 1. Overview Brahmaputra basin; the digital elevation model, location of the CRU TS2.1 grid points of the three physiographic zones, the discharge station at Bahadurabad and country boundaries. This figure is available in colour online at www.interscience.wiley.com/ijoc

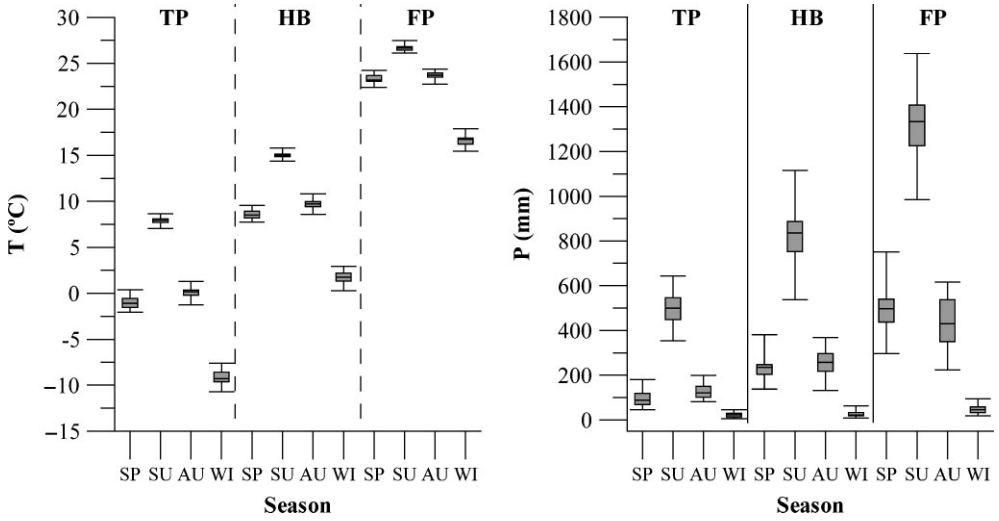

Figure 2. Box-whisker plot with seasonal climate normals (1961–1990) of temperature and precipitation for the three different physiographic zones (SP = spring (March, April, May), SU = summer (June, July, August), AU = autumn (September, October and November), WI = winter (December, January, February)).

average temperatures ranging from −10 °C in winter to 7 °C in summer. Winter temperatures in the HB fluctuate around 2 °C, while summer temperatures reach values of approximately 15 °C on average. The FP is the warmest of the three zones with winter temperatures around 17 °C and summer temperatures on average as high as 27 °C. For all zones the seasonal temperature variation is largest in winter and smallest in summer. The annual rainfall is concentrated in the monsoon months June, July, August and September (JJAS) in all zones. The TP located in the rain shadow of the HP is the driest zone in the basin (734 mm/year), while the FP is the wettest with an annual precipitation of 2354 mm. The HB has an average annual precipitation of 1349 mm.

Mountains are a major climate determinant and large-scale orography has a pronounced effect on atmospheric

Copyright © 2007 Royal Meteorological Society

DOI: 10.1002/joc

flow patterns. A precise understanding of the spatial and temporal behaviour of climate parameters and their projected change in mountain areas is hampered by the lack of observational data in complex topographic terrain and the difficulties to represent large mountain ranges in general circulation model (GCMs) (Beniston *et al*., 1997). Especially predicting changes in precipitation patterns in mountains pose additional challenges due to the inadequate representation of the local effects of topography on precipitation in most GCMs (Beniston, 2003). In addition to this, there is an intricate set of natural climate determinants that are known to influence the Asian monsoon; the El Niño – Southern Oscillation (ENSO) condition and the Eurasian snow depth levels. The relation between the monsoon and ENSO has been explored by numerous studies (Ropelewski and Halpert, 1989; Walker, 1924; Webster *et al*., 1999). The general consensus is that during El Niño years anomalous subsidence suppresses convection over South Asia and this results in a weaker monsoon (Krishna Kumar *et al*., 1999). Snow pack levels, specifically on the TP, also play a critical role in the variation in inter-annual precipitation. Upper-tropospheric air temperatures above the TP are among the warmest on the planet because of the heating of the elevated land with altitudes of over 3500 m. The troposheric temperature gradient between the TP and the Indian Ocean is shown to be associated with the Indian monsoon rainfall (Fu and Fletcher, 1985). The snow depth on the TP affects the land surface thermodynamics and reduces this thermal gradient. Shaman *et al*. (2005) report an inverse relationship between the spring snow depth on the TP and monsoon precipitation in Bangladesh. This does however not necessarily mean that these factors have influence on the precipitation in the entire Brahmaputra basin and this is subject of this study.

Climate change will have effects on the hydrology of the Brahmaputra basin. Large parts of the basin depend on the Brahmaputra discharge for irrigation while the lower part of the basin is vulnerable to flooding. Especially Bangladesh suffered severe flooding in 1987, 1988 and 1998 (Mirza, 2003). Climate change will affect the discharge characteristics significantly and will lead to more severe and more frequent flooding (Warrick *et al*., 1996) both through alterations in climatic conditions and sea level rise. Projected rise in temperature will lead to increased glacial and snow melt, which could lead to increased summer flows in some river systems for a few decades, followed by a reduction in flow as the glaciers disappear and snowfall diminishes. Satellite records have shown a decrease in snow cover extent of about 10% in the Northern hemisphere related to temperature increases in spring and summer since 1966 (Robinson, 1997, 1999). To what extent increased glacial and snow melt influence stream flow is varying strongly in space. Barnett *et al*. (2005) argue in a global study that the Hindu Kush Himalaya (HKH) region is the most critical area in which increased melt will affect water supply in the decades ahead. Within the Himalayan region there are however large differences in the contribution of melt water in total annual run-off. Rees and Collins (2006) show that the melt water component in the total run-off rapidly decreases rapidly from west to east. Summer precipitation declines from east to west. In the western Himalayas in winter at high elevations westerly winds provide precipitation while at lower altitudes arid conditions prevail. Total annual precipitation follows the east to west gradient. Therefore stream flow in basins in the west is for a major part determined by melt water while in the east run-off generated by monsoonal precipitation is the most important constituent of downstream discharge. Rees and Collins (2006) also argue that glaciers experience winter accumulation and summer ablation in the west, but there is predominantly synchronous summer accumulation and summer melt in the east. Singh and Bengtsson (2004) confirm the strong dependence of stream flow on melt water in basins originating in the western part of the basin and stress the difference in melt water contribution to stream flow between rain fed, snow fed and glacial fed river basins. The Brahmaputra basin is located in the eastern Himalayas and river discharges are predominantly rain fed.

Basin wide quantified assessments of climate change and its effects in the entire drainage area of the basin are scarce and not straightforward. Previous work indicates that specifically the TP is extremely sensitive to global climate change (Liu and Chen, 2000). A complete overview of the functioning of the Brahmaputra basin including the impact of climate change on run-off is lacking so far. Therefore this paper will focus on (1) analysis of historical trends in precipitation and temperature, (2) future trends in precipitation and temperature, and (3) the impact of climate change on hydrology.

2. Data and methods

Temperature and precipitation patterns were obtained using the most accurate global database currently available: the climate research unit (CRU) dataset. The latest updated version, referred to as the CRU TS 2.1 dataset in this paper, is used to reconstruct the temperature and precipitation patterns in the basin from 1901–2002 (Mitchell and Jones, 2005). The CRU TS 2.1 is a set of monthly climate grids which are constructed for nine climate variables and interpolated onto a 0.5° grid and provide best estimates of month-by month variations. The raw station data are derived from seven different sources and are corrected for in-homogeneities using a modified version of the Global Historical Climatology Network (GHCN) method (Peterson *et al*., 1998). The centre of the grid cells of the CRU TS 2.1 dataset is shown in Figure 1.

The interpolated value of a certain grid cell depends on a number of surrounding stations within a correlation decay distance. These distances are 1200 km and 450 km for temperature and precipitation respectively. This does not mean that all stations within this range actually influence the gridded value but it refers to the number of stations with information upon which the grid-box

Copyright © 2007 Royal Meteorological Society

DOI: 10.1002/joc

may draw, if necessary (New *et al*., 2000). The average number of stations in the basin within the correlation decay distance for each grid cell for precipitation and temperature are shown in Figure 3. Although this is the most accurate dataset available, the figure shows that some caution is required when interpreting data between 1901 and 1950 and after 1995.

Estimating future precipitation patterns requires understanding of current and past causes of precipitation processes. It is expected that precipitation in the basin is related to ENSO conditions and the thermal gradient between the FP and the TP. To explain precipitation patterns linear regressions were performed to identify relations between the monthly JJAS monsoon precipitation in the TP, the HB and the FP and the Southern Oscillation Index (SOI) (Können *et al*., 1998), the NINO3 index (Rayner *et al*., 2003) and the temperature difference between the FP and the TP (ΔT_{FP-TP}).

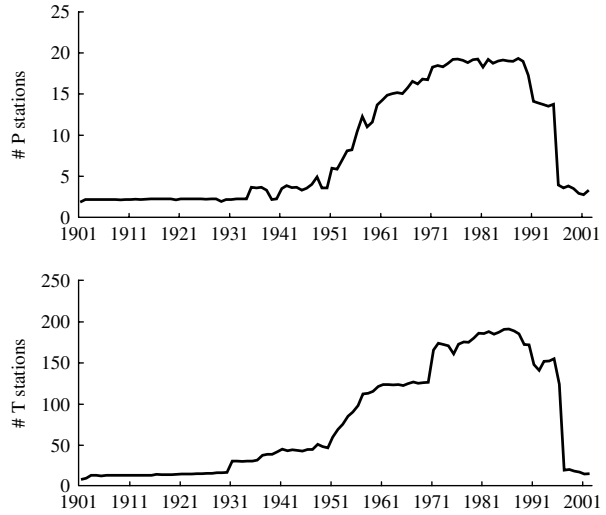

Figure 3. Average number of meterological stations in within the correlation decay distance for precipitation (left figure) and temperature (right figure).

GCM monthly precipitation and temperature fields from six different models from 2002 to 2100 are used to analyse the A2 and B2 storylines (Parry, 2002). GCM data were downloaded from the IPCC Data Distribution Centre (IPCC-DDC, http://ipcc-ddc.cru.uea.ac.uk/). Table I shows that the different GCMs have a varying spatial resolutions typically in the range of three degrees. In order to capture basin scale variations in temperature and precipitation and the large-scale behaviour of the GCMs a statistical downscaling procedure is applied. The GCM outputs are downscaled to the resolution of the CRU TS 2.1 dataset (0.5° by 0.5°) using a similar procedure as Bouwer *et al*. (2004). This method ensures conservation of the variability and mean during the reference period.

The average seasonal anomalies (2061–2090 compared to 1961–2000) in precipitation and temperature are determined at the centres of the CRU TS 2.1 grid cells. These anomalies are spatially interpolated to a resolution of 0.05° using a spline tension interpolator with weight one using four CRU TS 2.1 points. This interpolator ensures a smooth (continuous and differentiable) surface, together with continuous first-derivative surfaces (Franke, 1982). This approach is appropriate to assess spatial climate patterns at basin scale.

Daily discharge data at the Bahadurabad gauging station (Figure 1) from 1956 to 1993 were analysed using a multiple regression based rainfall-run-off model. Average monthly hydrographs in combination with monthly precipitation were assessed on the contribution of snow melt to annual stream flow. Only if there is sufficient reason to assume that the majority of stream flow is related to rainfall it is legitimate to use a multiple regression run-off model using rainfall data.

Table I. Overview of the GCMs used, the reference periods and latitudinal and longitudinal spatial resolutions.

Model	Institute	Acronym	Reference period	Latitudinal resolution	Longitudinal resolution
CCSR	Japanese centre for climate system research, Tokyo, Japan	CCS	1890–2002	~5.54°	~5.63°
CGCM2	Canadian centre for climate modelling and analysis, Victoria, Canada	CGC	1900–2002	~3.71°	~3.75°
CSIRO-Mk2	Australian commonwealth scientific and industrial research organisation, Australia	CSI	1961–2002	~3.19°	~5.63°
ECHAM4/OPYC3	Max-Planck-institute, Hamburg, Germany	EH4	1990–2002	~2.79°	~2.81°
GFDL-R30	US geophysical fluid dynamics laboratory, Princeton, USA	GFD	1961–2002	~2.24°	~1.88°
HADCM3	Hadley centre for climate prediction and research, Bracknell, UK	HAD	1950–2002	~2.50°	~3.75°

Copyright © 2007 Royal Meteorological Society

DOI: 10.1002/joc

Multiple linear regression was used to model average monthly stream flow in month t using three variables; basin precipitation in month t (P_t (mm)), basin precipitation in month $t-1$ (P_{t-1}(mm)) and ΔT_{FP-TP}(°C) in month t. To capture seasonal variation regression models were derived for summer, winter, autumn and spring separately. These models are of the form:

Equation

$$\mathbf{Q}_{avg} = a + b1 \cdot P(t) + b2 \cdot P(t-1) + b3 \cdot \Delta T_{FP-TP} \quad (1)$$

where Q_{avg} (m^3/s) is the average monthly discharge, a is the intercept and *b1, b2* and *b3* are coefficients. Based on these models and the downscaled data of six GCMs, seasonal models with monthly time series of average discharges has been generated for the A2 and B2 storylines from 1901 to 2100.

3. Results

3.1. Historical trends

Figure 4 shows the anomalies in temperature and precipitation from 1900 to 2002 for the three physiographic zones. Six extreme warm years (10% warmest years) have occurred between 1995 and 2002. For the TP, HB and the FP temperature patterns are remarkably consistent with the global warming pattern. The warming trend is obvious throughout the entire basin at an average rate of 0.6 °C/100 year. Figure 4 does not reveal any large difference between the different zones in annual temperature trends. The TP reveals most inter-annual variation. There are however seasonal differences. All zones show the largest warming trend in spring (TP = 1.1 °C/100 year, HB = 1.0 °C/100 year, FP = 0.9 °C/100 year) and the smallest warming trend in summer (TP = 0.2 °C/100 year, HB = 0.4 °C/100 year, FP = 0.5 °C/100 year). There is an obvious difference between the zones in summer temperature trend. Annual trends in precipitation are not observed from 1901

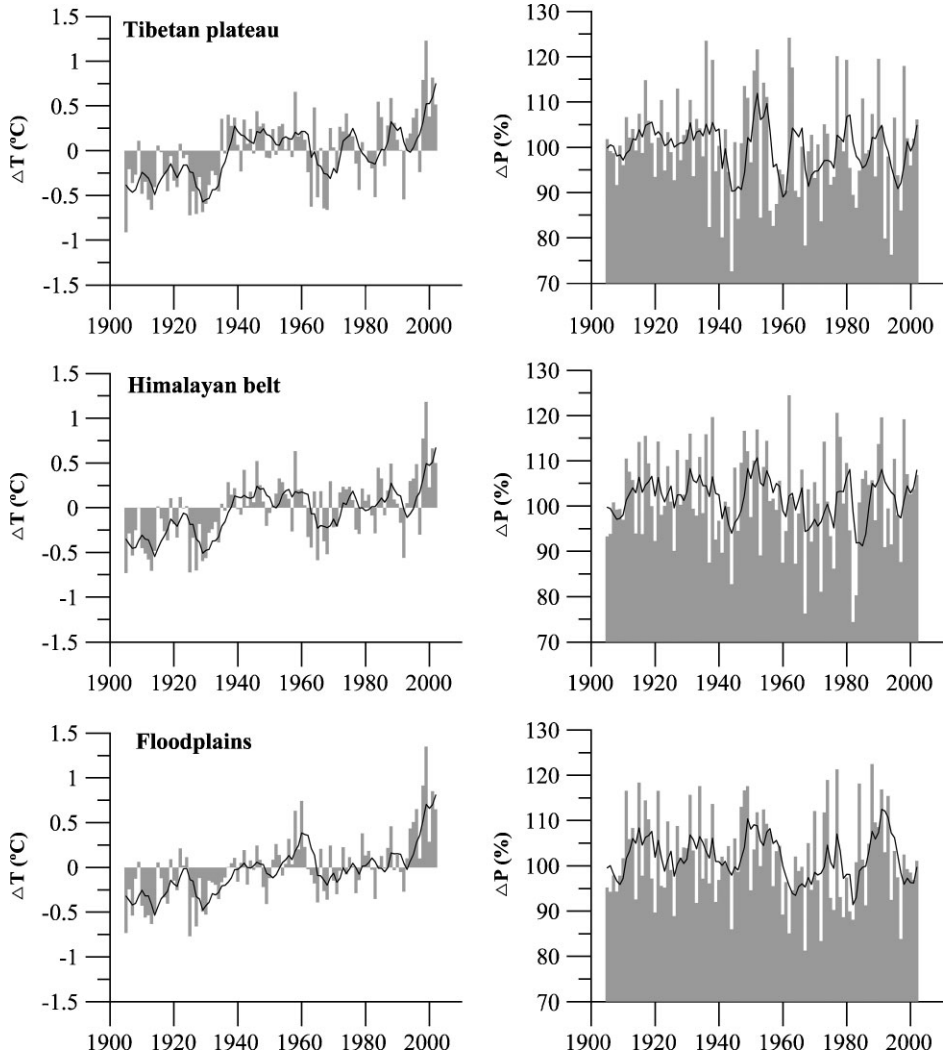

Figure 4. Temperature anomalies (Δ °C) (left) and precipitation anomalies (%) (right) per physiographic zone from 1905 to 2002. The lines indicate the 5 year moving average of temperature and precipitation anomalies from the climate normal 1961–1990. The bars in the temperature graphs (left) indicate the original year temperature and precipitation anomalies respectively.

Copyright © 2007 Royal Meteorological Society

DOI: 10.1002/joc

to 2002. The precipitation pattern in all three zones does not show any resemblance to the global precipitation anomalies, which exhibit a slight positive trend. An approximate 15 year cycle in the annual precipitation pattern is observed. The TP and HB show most inter-annual variation. Other factors evidently play an important role in the inter-annual variation in precipitation. The winter precipitation trends are positive for all zones (TP = 6.7%/100 year, HB = 6.1%/100 year, FP = 7.5%/100 year), while in summer there is a general negative trend for all zones (TP = −6.3%/100 year, HB = −4%/100 year, FP = −5.2%/100 year). Autumn precipitation trends are also positive which could indicate a delay in the onset of the monsoon.

The annual precipitation patterns in the basin are further explained by linear regression analysis. Figure 5 shows the results of the linear regressions between the JJAS zonal precipitation and SOI, NINO3 and ΔT_{FP-TP} respectively. The ENSO indices do not have a prominent role in explaining the JJAS precipitation in all three zones, and the correlations found are negligible. A significant relation is however found between ΔT_{FP-TP} and the monsoon precipitation, ranging from $R^2 = 0.32$ on the TP to $R^2 = 0.42$ on the FP. Regression analysis between ΔT_{FP-TP} and total JJAS basin precipitation results in an R^2 of 0.45. This leads to the interesting finding that precipitation in the basin is inversely related to the gradient in surface air temperatures between the FP and TP. A small ΔT_{FP-TP} is associated with relatively high air temperatures on the TP and low air temperatures in the FP. This is indicative of increased warming of the TP land surface and the atmosphere above.

3.2. Future changes

Figure 6 shows the downscaled temperature and precipitation anomalies from 2000 to 2100 per physiographic zone. The graphs show the average of all six GCMs. The HADCM3 model is an intermediate model in all projections in all zones. For both temperature and precipitation the HADCM3 model shows the best downscaling results in maintaining the time series characteristics during the reference period, specifically variation in precipitation.

The coefficient of variation between the six GCMs in precipitation is on average 9% and the standard deviation in temperature between the GCMs is 0.5 °C for both storylines. There is a slight increasing trend in variation from 2000 to 2100.

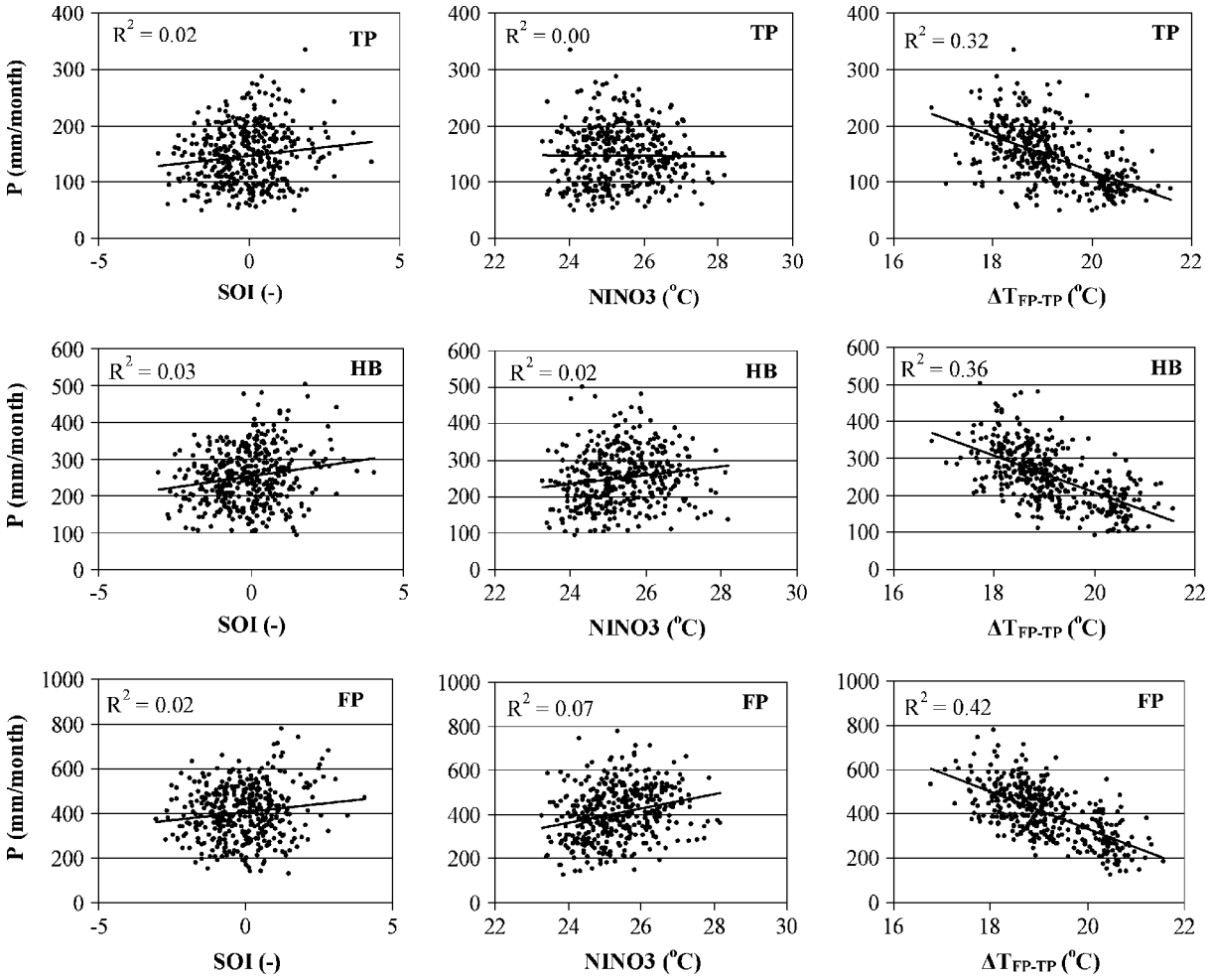

Figure 5. Linear regressions for the TP, HB and FP between monthly precipitation in June, July, August and September and SOI, NINO3 and the FP−TP temperature difference for the period 1901–2002.

Copyright © 2007 Royal Meteorological Society

DOI: 10.1002/joc

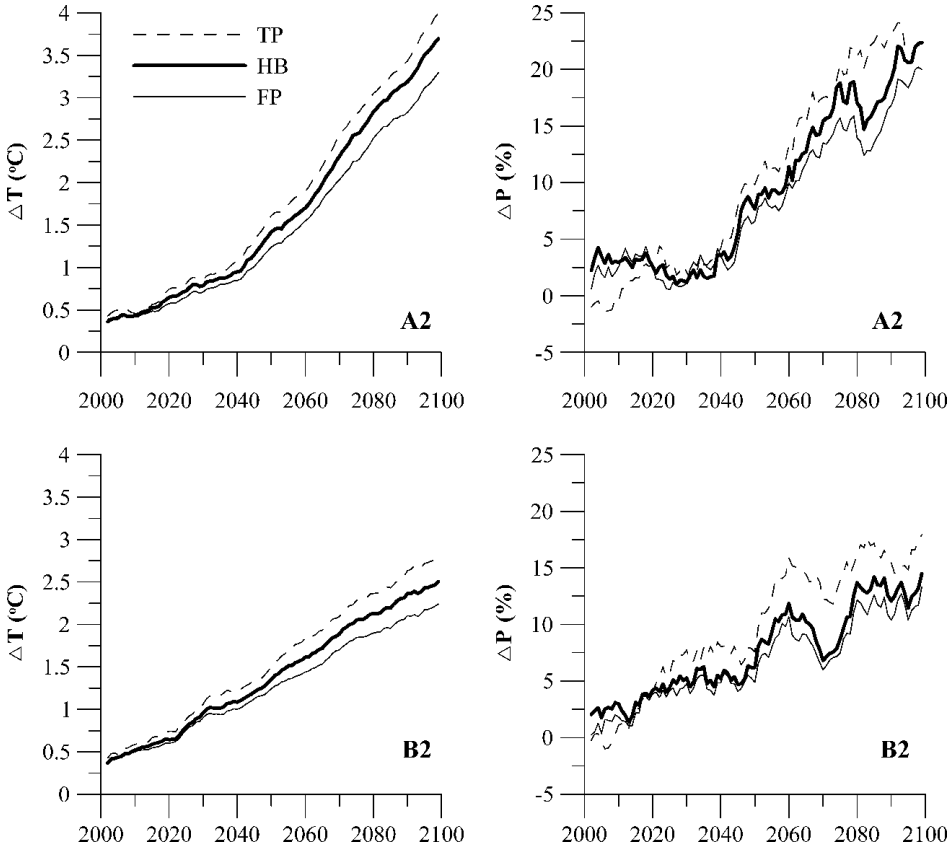

Figure 6. Downscaled temperature and precipitation anomalies from the climate normal 1961–1990 based on the average of six GCMs from 2002 to 2100 per physiographic zone.

By the end of the century the A2 storyline shows more extreme changes in precipitation and temperature than the B2 storyline. By 2100 it is projected that on average the temperature in the basin has increased by 3.5 and 2.3 °C for the A2 and B2 storylines respectively. The projected changes in precipitation show a more capricious pattern but a consistent increase of 22% and 14% by 2100 for the A2 and B2 storyline respectively is observed. The dips in the precipitation time series at 2080 for the A2 scenario and 2070 for the B2 scenario are caused by anomalous behaviour of the CGC GCM. For both temperature and precipitation inter-zonal differences are evident and the TP is the most sensitive to climate change, followed by the HB and the FP for the A2 and B2 storylines. This also means that ΔT_{FP-TP} will decrease because the TP warms at a faster pace than the FP.

The box-whisker plots in Figure 7 shows the basin seasonal shifts in temperature and precipitation. The seasonal climate normals (1961–1990) are compared to 2061–2090 for the A2 and B2 storylines. Data of a single GCM (HADCM3) are used to be able to analyse changes in variation. All seasons show an increase in temperature, which is more pronounced for the A2 scenario than the B2 scenario, except for winter when both scenarios show a similar increase. Autumn shows the largest difference in temperature increase between the two storylines. The difference between the first and third quartiles in summer has increased for both storylines resulting from a wider distribution in temperatures. Seasonal precipitation trends are also positive except for autumn and summer precipitation for the B2 storyline which have the median lower than the 1961–1990 value. The frequency distribution of precipitation is generally widened and the extreme values, especially in summer have increased.

The spatial patterns in the basin are revealed by the spatially interpolated temperature and precipitation maps in 2020, 2050 and 2080 for the A2 and B2 storylines in Figures 8 and 9. The TP, specifically the north eastern part shows the largest increase in temperature. Both storylines show similar spatial behaviour and significant spatial differences in temperature between the scenarios become apparent after the 2050's. The Himalayas obviously have a pivotal role in the regional climate system and temperature anomalies generally follow the orography.

The spatial precipitation patterns (Figure 9) also shows the strongest increase in precipitation on the TP and the least increase in the FP. The total amount of precipitation in the FP is however more than three times as large than in the TP. The spatial patterns are more capricious than the spatial patterns in temperature. There is a distinct horizontal band around 29 °N south of the Brahmaputra River, which shows a remarkably steep increase in

Copyright © 2007 Royal Meteorological Society

DOI: 10.1002/joc

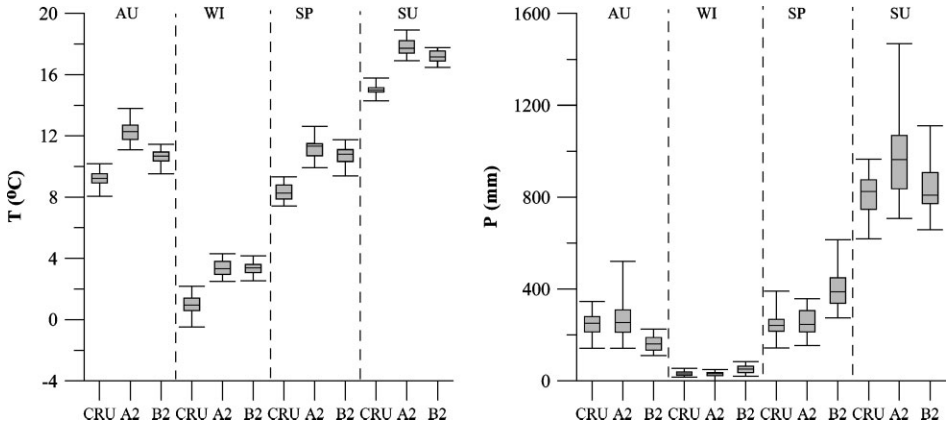

Figure 7. Box-whisker plot of seasonal temperatures and precipitation for observed data and HADCM3 climate change predictions for the A2 and B2 scenario (CRU = CRU TS2.1 1961–1990, A2 = downscaled HADCM3 results 2061–2090 for the A2 scenario, B2 = downscaled HADCM3 results 2061–2090 for the B2 scenario).

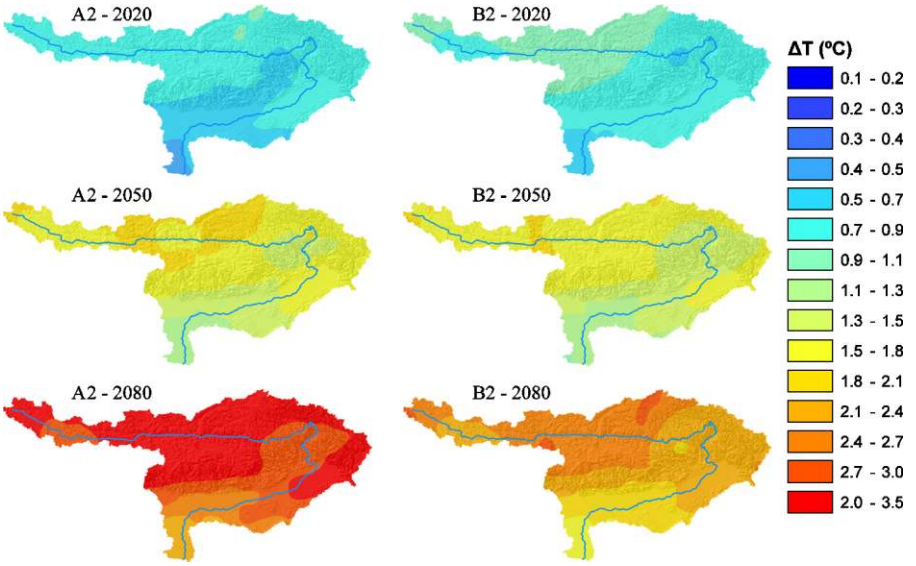

Figure 8. Downscaled spatial temperature anomalies from the climate normal 1961–1990 based on the average of six GCMs for the 2020 (2010–2030), 2050 (2040–2060) and 2080 (2070–2090). This figure is available in colour online at www.interscience.wiley.com/ijoc

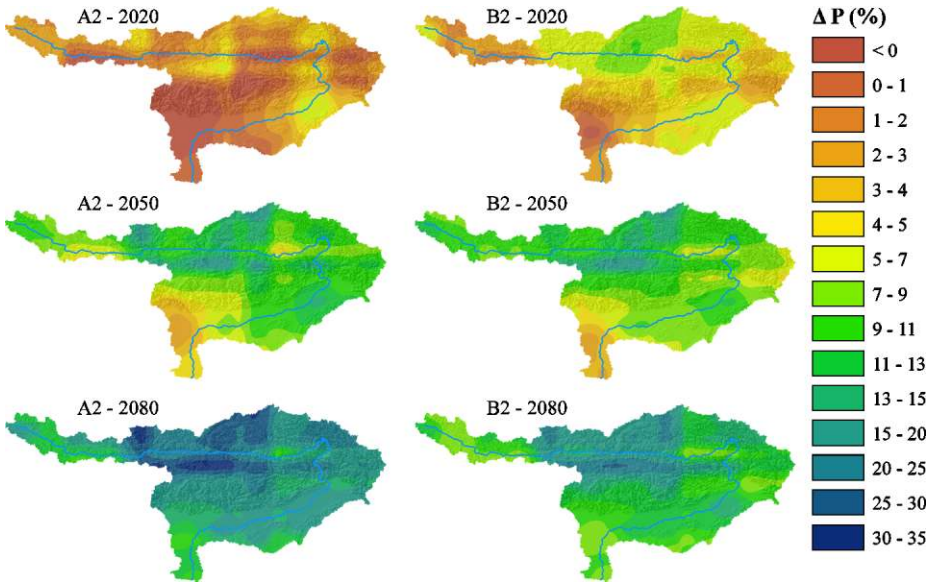

Figure 9. Downscaled spatial precipitation anomalies from the climate normal 1961–1990 based on the average of six GCMs for the 2020 (2010–2030), 2050 (2040–2060) and 2080 (2070–2090). This figure is available in colour online at www.interscience.wiley.com/ijoc

Copyright © 2007 Royal Meteorological Society

DOI: 10.1002/joc

precipitation in all years for both storylines. This amounts to a precipitation increase to over 30% in the 2080's for the A2 storyline. The A2 storyline in 2020 shows for large parts of the HB and the FP a remarkable decrease in precipitation. The effects of the Himalayas are also visible in the spatial precipitation patterns.

3.3. Hydrological impacts

Figure 10 shows the average monthly hydrograph based on daily discharge data from 1956 to 1993. The hydrograph and scatter plot show that stream flow at Bahadurabad is mainly generated by rainfall. The scatter plot reveals that from the end of the monsoon onwards, when soils are saturated, discharge is relatively high. In the early spring months when soils have not yet reached saturation, discharge is relatively low. The hydrograph shows that discharge responds directly to rainfall with a typical lag of one month and there is no additional peak in spring related to snow and glacial melt. This does comply with earlier studies that report synchronous accumulation and melt in eastern Himalayan basins (Rees and Collins, 2006). In addition to this summer precipitation in all zones is much larger than winter precipitation in the TP and HB (Figure 2). Therefore it may be concluded that the overall contribution of snow and glacial melt to downstream discharge in the Brahmaputra will be very small and that it is legitimate to use a simple rainfall-run-off model to gain insight in stream flow patterns. The total average annual precipitation sum between 1956 and 1993 is 1336 mm, while total discharge is on average 1200 mm.

Table II shows the results of the seasonal regression models. All seasons, except winter, show good results with R^2 ranging from 0.64 in summer to 0.82 in autumn and spring. Winter discharges show limited response to P_t, P_{t-1} and ΔT_{FP-TP}, while average discharge is also relatively low. P_t and P_{t-1} are proportional and ΔT_{FP-TP} is inversely proportional to Q_{avg} in all cases where significant contributions are found.

Using the regression models and the average monthly P_t, P_{t-1} and ΔT_{FP-TP} of the six GCMs the seasonal effects on the discharge from 200 to 2100 are determined (Figure 11). During the monsoon in summer the strongest increase in discharge is expected and projections range between 20% and 30% increase of average monthly discharge for the B2 and A2 scenarios respectively.

Table II. Seasonal regression models for average discharge at Bahadurabad based on data from 1954 to 1992. Q_{avg} is the average discharge from 1954 to 1992. R^2 is the multiple R squared, a is the intercept and *b1, b2* and *b3* are the coefficients in equation 1. A '*' indicates significant contribution at the 95% confidence level.

	Autumn	Winter	Spring	Summer
Q_{avg} (m^3/s)	25 267	5518	9247	40 204
R^2	0.82	0.06	0.82	0.64
a	−254	14 275*	28 253*	73 630*
b1	97*	−10	35*	72*
b2	73*	33	38*	68*
b3	242	−347*	−964*	−3635*

Winter discharges show little change and discharge is mainly fed by groundwater base flow. Autumn and spring show intermediate increases in discharge. The increase in summer is critical and this will most likely also entail an increase in the number of extreme discharges, since there is a strong relation between average monthly discharge and maximum monthly discharge ($R^2 = 0.61$; Figure 12).

4. Discussion and Conclusions

The historical analysis of precipitation and temperature revealed that there is a clear increasing trend in temperature at an average rate of 0.6 °C/100 year, with the largest increases in spring. No distinct drying or wetting trends are observed over the last 100 year and annual precipitation is primarily controlled by monsoon dynamics.

The GCM simulations show an accelerated increase in both temperature and precipitation. Projected changes on the TP are more profound than in the other two physiographic zones. The widening distribution of summer precipitation indicates a potential increase in extreme events.

In this paper an analysis is provided of the historical climatic variations at the scale of a large river basin. The CRU TS 2.1 dataset is not always suitable to provide time series analysis at the scale of an individual grid box. The grids are optimized in space rather than in time, resulting in instantaneous best estimates of spatial patterns. The analysis also revealed a large variation in time in the

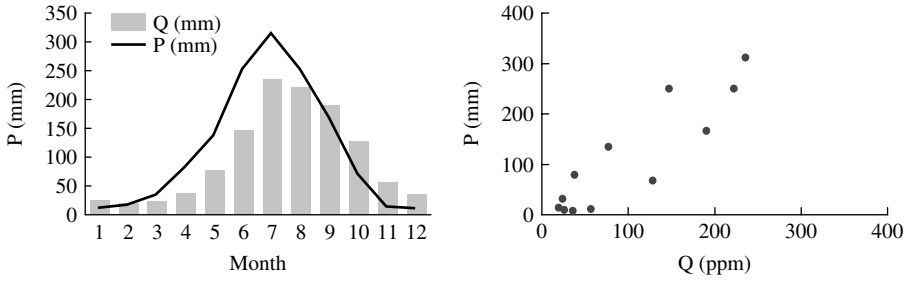

Figure 10. Average monthly hydrograph at Bahadurabad and basin precipitation (left figure) and scatter plot between monthly basin precipitation and Bahadurabad discharges (right figure) (1956–1993 data).

Copyright © 2007 Royal Meteorological Society

DOI: 10.1002/joc

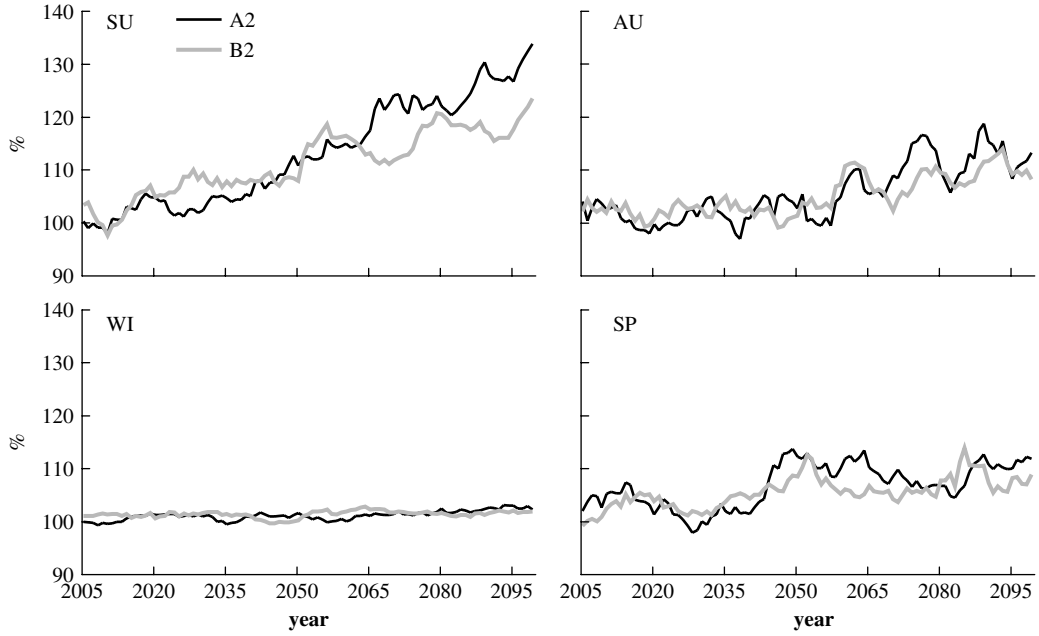

Figure 11. Projected trends in seasonal discharges at Bahadurabad based on multiple linear regression models and average data of six GCMs.

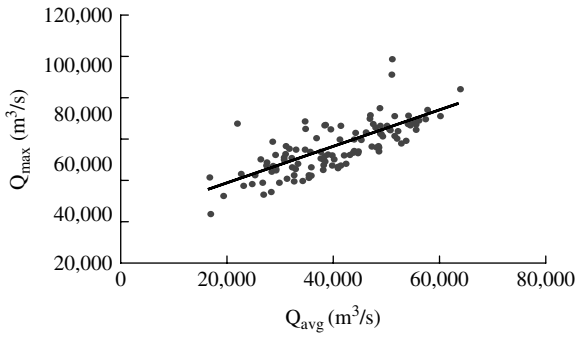

Figure 12. Relation between monthly average and extreme discharges at Bahadurabad.

number of stations within the correlation decay distance. For these reasons the time series analysis conducted in this research on the dataset was mainly conducted per physiographic zones and problems caused by local inhomogeneities at a specific location were avoided.

The historical analysis showed clear temperature trends, however no clear trends in precipitation were observed although seasonal variations were apparent. This study reveals no significant relation between ENSO and monsoon precipitation, which is not in agreement with earlier findings (Krishna Kumar *et al*., 1999) and should be subject to further research. A large part of the variation in monsoon precipitation is however explained by the surface air temperature gradients between the FP and the TP. Relatively high temperatures on the TP and low temperatures on the FP generally yield stronger monsoons. Previous studies (Barnett *et al*., 1989; Shaman and Tziperman, 2005) argue how thermodynamics on the TP reduce the strength of the monsoon through a decrease of the upper-tropospheric temperature gradient between TP and the Indian Ocean. They argue that the reduction of the thermal gradient is caused by an increased TP snow pack resulting in a number of thermodynamic effects which all result in lower air temperatures of the atmosphere above the TP; (1) an increased snow pack yields a higher albedo leaving less solar radiation for the sensible heat flux, (2) of the energy which is left a substantial part is required for sublimation and (3) the melting of the snow leaves a wetted surface and a large part of the energy is consumed by the latent heatflux. In other words low air temperatures on the TP (= high ΔT_{FP-TP}) generally yield weak monsoons, which is in agreement with findings of this study. Kripalani *et al*. (2004) found that the well-documented negative relationship between winter snow and summer rainfall has recently changed into a positive relation ship in the western Himalayas, and argue that a possible cause might be found in global warming and the interaction between snow depth and cover.

The future precipitation increase simulated by the GCMs is assumed to be driven by global warming rather than changes in atmospheric dynamics. The study revealed an inverse relation between ΔT_{FP-TP} and precipitation. The GCM analysis showed that this gradient will decrease in the years ahead, which would result in higher precipitation according to the relation found.

To which extent remains however largely unknown and this should be topic of future research and some caution is warranted. A number of recent studies have, for example, investigated the influence of black carbon aerosols on the South Asian monsoon, suggesting a competing effect with increasing concentrations of greenhouse gases (Lau *et al*., 2006; Ramanathan *et al*., 2005; Ramanathan and Chung, 2006). These specific aerosols are not included in the climate models.

The hydrological analysis showed that it is likely to assume that the majority of downstream stream flow in the Brahmaputra is generated by rainfall and to a

Copyright © 2007 Royal Meteorological Society

DOI: 10.1002/joc

much lesser extent by snow and glacial melt. It was also found that the average difference between annual precipitation and discharge only leaves 136 mm for ET. Assuming that the soil water storage balance is close to zero this is not realistic given the high potential ET rates. The logical explanation is that the CRU precipitation, based on a limited number of stations, underestimates the precipitation in the floodplain due to orographic effects in the Meghalaya hills and the Himalayan foothills. Nijssen *et al*. (2000) found similar results. Through relative simple multiple regression analysis interesting relations are found between JJAS discharges and precipitation. It showed that trends in average and extreme discharges can be reasonably well predicted, but that the most extreme discharge events are missed by the regression model. There are several potential reasons. Extreme discharges are often the result of precipitation events with a daily timescale. Extreme discharges at Bahadurabad are combination of processes and the upstream hydro-meteorological processes are not the only cause for floods in Bangladesh. The combination of simultaneous discharge peaks of the tributaries, high run-off from the Meghalaya Hills, heavy rainfall in Bangladesh, high groundwater tables and spring tides will results in a very high peak discharges at Bahadurabad (Messerli and Hofer, 2006).

In this research direct relationships with zonal precipitation were investigated. This study provides a baseline against which process based hydrological models may be built and used to simulate the complete anticipated effects on the hydrological cycle. Changes in snowfall, ET and groundwater recharge can thus be modelled and related to food production in a changing environment.

Acknowledgements

The author is grateful to Dr. P.D. Mitchell and Dr. T.D. Jones of the University of East Anglia for providing the high resolution CRU TS 2.1 dataset (Mitchell and Jones, 2005), to Dr. T. Islam of the Institute of Water and Flood Management Bangladesh University of Engineering and Technology for providing the discharge data of Bangladesh and to the IPCC-DDC for providing the interface for downloading the GCM data. The author is also grateful to two anonymous reviewers for providing valuable comments.

References

Arnell NW. 1999. Climate Change and global water resources. *Global Environmental Change* **9**: 31–49.

Barnett TP, Adam JC, Lettenmaier DP. 2005. Potential impacts of a warming climate on water availability in snow-dominated regions. *Nature* **438**: 303–309, DOI 10.1038/nature04141.

Barnett TP, Dumenil L, Schlese U, Roeckner E, Latif M. 1989. The effect of Eurasian snow cover on regional and global climate variations. *Journal of the Atmospheric Sciences* **46**: 661–685.

Beniston M. 2003. Climatic Change in mountain regions: a review of possible impacts. *Climatic Change* **59**: 5–31.

Beniston M, Diaz HF, Bradley RS. 1997. Climatic Change at high elevation sites: an overview. *Climatic Change* **36**: 233–251.

Bouwer LM, Aerts JCJH, van de Coterlet GM, van de Giesen N, Gieske A, Mannaerts C. 2004. Evaluating downscaling methods for preparing Global Circulation Model (GCM) Data for Hydrological Impact Modelling. In *Climate Change in Contrasting River Basins*, Aerts JCJH, Droogers P (eds). CABI Publishing: Wallingford.

Franke R. 1982. Smooth interpolation of Scattered data by local thin plate splines. *Computers and Mathematics with Applications* **8**: 237–281.

Fu C, Fletcher JO. 1985. The relationship between Tibet tropical ocean thermal contrast and the interannual variability of Indian monsoon rainfall. *Journal of Climate and Applied Meterology* **24**: 841–847.

IPCC. 2001. *Climate Change 2001: The Scientific Basis*. Cambridge University Press: Cambridge.

Können GP, Jones PD, Kaltofen MH, Allan RJ. 1998. Pre-1866 extensions of the Southern Oscillation Index using early Indonesian and Tahitian meteorological readings. *Journal of Climate* **11**: 2325–2339.

Kripalani RH, Kulkarni S, Sabade S. 2004. Western Himalayan snow cover and Indian monsoon rainfall: A re-examination with INSAT and NCEP/NCAR data. *Theoretical and Applied Climatology* **74**: 1–18.

Krishna Kumar K, Rajagopalan B, Cane MA. 1999. On the weakening relationship between the Indian monsoon and ENSO. *Science* **284**: 2156–2159.

Lau KM, Kim MK, Kim KM. 2006. Asian summer monsoon anomalies induced by aerosol direct forcing: the role of the Tibetan Plateau. *Climate Dynamics* **26**: 855–864.

Liu X, Chen B. 2000. Climatic Warming in the Tibetan Plateau during recent decades. *International Journal of Climatology* **202**: 1729–1742.

Messerli B, Hofer T. 2006. *Floods in Bangladesh: History, Dynamics and Rethinking the Role of the Himalayas*. United Nations University Press: Tokyo.

Mirza MMQ. 2003. Three recent extreme floods in Bangladesh: A hydro-meteorological analysis. *Natural Hazards* **28**: 35–64.

Mitchell TD, Jones PD. 2005. An improved method of constructing a database of monthly climate observations and associated high-resolution grids. *International Journal of Climatology* **25**: 693–612, DOI 10.1002/joc.1181.

New M, Hulme M, Jones P. 2000. Representing Twentieth-Century Space–Time climate variability. Part II: development of 1901–96 monthly grids of terrestrial surface climate. *Journal of Climate* **13**: 2217–2238.

Nijssen B, O'Donnel GM, Lettenmaier DP, Lohmann S, Wood EF. 2000. Predicting discharge of global rivers. *Journal of Climate* **14**: 3307–3322.

Parry M. 2002. Scenarios for climate impact and adaptation assessment. *Global Environmental Change* **12**: 149–153.

Peterson TC, Easterling DR, Karl TR, Groisman P, Nicholls N, Plummer N, Torok S, Auer I, Boehm R, Gullett D, Vincent L, Heino R, Tuomenvirta H, Mestre O, Szentimrey T, Salinger J, Forland E, Hanssen-Bauer I, Alexandersson H, Jones P, Parker D. 1998. Homogeneity adjustments of in situ atmospheric climate data: a review. *International Journal of Climatology* **18**: 1493–1517.

Ramanathan V, Chung C. 2006. Weakening of North Indian SST Gradients and the Monsoon Rainfall in India and the Sahel. *Journal of Climate* **19**: 2036–2045.

Ramanathan V, Chung C, Kim D, Bettge T, Buja L, Kiehl JT, Washington WM, Fu Q, Sikka DR, Wild M. 2005. Atmospheric brown clouds: Impacts on S. Asian climate and hydrological cycle. *Proceedings of the National Academy of Sciences (PNAS)* **102**: 5325–5333, DOI: 10.1073/pnas.0500656102.

Rayner NA, Parker DE, Horton EB, Folland CK, Alexander LV, Rowell DP, Kent EC, Kaplan A. 2003. Global analyses of sea surface temperature, sea ice, and night marine air temperature since the late nineteenth century. *Journal of Geophysical Research* **108**(D14): 4407, DOI: 10.1029/2002JD002670.

Rees HG, Collins DN. 2006. Regional differences in response of flow in glacier-fed Himalayan rivers to climatic warming. *Hydrological Processes* **20**: 2157–2169.

Robinson DA. 1997. Hemispheric snow cover and surface albedo for model validation. *Annals of Glaciology* **25**: 241–245.

Robinson DA. 1999. Northern Hemisphere snow cover during the satellite era. In *Proceedings of the 5th Conference on Polar Meteorology and Oceanography*, Dallas, Texas, USA, 255–260.

Ropeleweksi CF, Halpert MS. 1989. Precipitation patterns associated with the high index phase of the Southern Oscillation. *Journal of Climate* **2**: 268–284.

Shaman J, Tziperman E. 2005. The effects of ENSO on Tibetan plateau snow depth: A sationary Wave Teleconnection Mechanism and

Copyright © 2007 Royal Meteorological Society

Implication for the South Asian Monsoons. *Journal of Climate* **18**: 2067–2079.

Shaman J, Cane M, Kaplan A. 2005. The relationship between Tibetan snow depth, ENSO, river discharge and the monsoon of Bangladesh. *International Journal of Remote Sensing* **26**: 3735–3748, DOI 10.1080/01431160500185599.

Singh P, Bengtsson L. 2004. Impact of warmer climate on melt and evaporation for the rainfed, snowfed and glacierfed basins in the Himalayan region. *Journal of Hydrology* **300**: 140–155.

Walker GT. 1924. Correlation in seasonal variations of weather. IV. A further study of world weather. *Memoirs of the Indian Meteorological Department* **24**: 275–332.

Warrick RA, Bhuiya AH, Mirza MQ. 1996. The greenhouse effect and climate change. In *The Implications of Climate and Sea-Level Change for Banglades*, Warrick RA, Ahmad QK (eds). Kluwer Academic Publishers: Dordrecht.

Webster PJ, Moore AM, Loschnigg JP, Leben RR. 1999. Coupled ocean–atmosphere dynamics in the Indian ocean during 1997–98. *Nature* **401**: 356–360.

Copyright © 2007 Royal Meteorological Society